Dalton Transactions

Accepted Manuscript

ROYAL SOCIETY OF CHEMISTRY

www.rsc.org/dalton

Graphene Oxide Coated Coordination Polymer Nanobelt Composite Material: a New Kind of Visible Light Active and High Efficient Photocatalyst for Cr (VI) Reduction

Gui-Mei Shi,*[a] Bin Zhang,[a] Xin-Xin Xu,*[b] and Fu-Yang Hong[a]

[a] *College of Science, Shenyang University of Technology, No.111, Shenliao West Road, Economic & Technological Development Zone, Shenyang,110870,P. R. China*

[b] *Department of Chemistry, College of Science, Northeast University, Shenyang, Liaoning, 110819, People's Republic of China*

*Author to whom correspondence should be addressed.

E-mail: gmshi@imr.ac.cn (Professor G. M. Shi)

xuxx@mail.neu.edu.cn (Professor X. X. Xu)

Abstract

A visible light active photocatalyst was synthesized successfully through the coating of graphene oxide (**GO**) on coordination polymer nanobelt (**CPNB**) with a simple colloidal blending process. Compared with neat **CPNB**, the resulted graphene oxide coated coordination polymer nanobelt composite material (**GO/CPNB**) exhibits excellent photocatalytic efficiency on the reduction of $K_2Cr_2O_7$ under visible light irradiation. In composite material, **GO** performs two functions. At first, it cuts down band gap (E_g) of photocatalyst and extends its photoresponse region from ultraviolet to visible light region. Secondly, **GO** exhibits excellent electron transportation ability and impede its recombination with hole, which can enhance photocatalytic efficiency. For **GO**, on its surface, the number of functional group has great influence on photocatalytic performance of the resulted **GO/CPNB** composite material and an ideal **GO** "coater" to obtain high efficient **GO/CPNB** photocatalyst has been obtained. As a photocatalyst which may be used in the treatment of Cr(VI) in wastewater, **GO/CPNB** exhibited outstanding stability during the reduction of this pollutant.

Introduction

As a mutagenic, carcinogenic and notoriously toxic, hexavalent chromium (Cr(VI)) is wide disturbed in wastewater all over the world, since it is indispensable during many industrial processes.[1,2] Nowadays, the dire consequences caused by Cr(VI) pollution makes its cost-effective and low energy expending treatment highly desired.[3,4] In this aspect, photocatalytic reduction has been proved to be a promising method for the hypotoxic reduction product of this process, Cr(III).[5] Up to now, several semiconductor photocatalysts have been employed for photocatalytic reduction of Cr(VI) and researchers are exploring photocatalysts with more excellent performance.[6] As a type of new photocatalyst, coordination polymers (**CP**), especially nanoscale coordination polymers (**NCP**) have attracted considerable attention, owing to their potential application in green photocatalytic reduction of Cr(VI) and other pollutants.[7,8] Although a few ultraviolet-light-active **NCP** photocatalysts have been reported, the design and fabrication of visible-light-active **NCP** photocatalysts with high photocatalytic efficiency still remains a challenge, which surfers from drawbacks of wide band gap and flash electron-hole recombination rate during the photocatalysis process.[9-12]

For wide band gap photocatalysts such as **NCP**, to improve their photocatalytic activity, the combination with carbonaceous material is a feasible strategy because the formation of chemical bonds between **NCP** and carbonaceous material can decrease band gap and extend photoresponse region.[13] Furthermore, for its excellent electrical conductivity, carbonaceous material can transport electron in time and impede its recombination with hole. In the family of carbonaceous material, **GO** is an ideal choice.[14] Firstly, the functional groups (such as -COOH and -OH) on its surface can form chemical bonds with metal ion of **NCP**.[15] Secondly, as other carbonaceous

substance, **GO** is an excellent electron transporter, which can take electron away and shields it from hole.16 Thirdly, the large surface area and outstanding absorption capability make **GO** an ideal carrier for the fabrication of composite material.[17] To our knowledge, **GO** has been employed to improve the photocatalytic activity of some wide band gap photocatalysts and achieved satisfactory results.[18] Hence we speculate photocatalytic activity of **NCP** can also be improved through its combination with **GO**.

Our imagination was confirmed to be reasonable by a composite material, named as **GO/CPNB**, which was fabricated by the coating of **GO** on nanobelt of a new coordination polymer, $[Zn(cca)_2(bipy)]_n \cdot n(bipy)$ (**CP**) (cca = 4-carboxycinnamic dianion; bipy = 2,2'-bipyridine). Photocatalytic reduction of $K_2Cr_2O_7$ was investigated under visible light irradiation and the results indicated the coating of **GO** on **NCP** could enhance **NCP's** photocatalytic activity effectively. For **GO**, the number of functional group had great effects on its physical and chemical properties, which may further influence photocatalytic activity of **GO/CPNB**. Here, on **GO**, the number of functional group was controlled by the mass of oxidant. The influence of functional group on photocatalytic property had been discussed in detail.

Experimental Section

Materials and Synthesis

All purchased chemicals were of reagent grade and used without further purification. The morphology was observed on an ultra plus field emission scanning electron microscope (ZEISS, Germany). PXRD patterns were recorded on D8 X-ray diffractometer, employing monochromatized Cu Kα incident radiation. FTIR spectra were recorded in the range 4000-400 cm^{-1} on an Alpha Centaur FTIR spectrophotometer using KBr pellets. The X-ray photoelectron spectroscopy (XPS)

measurements were carried out on a Thermo Scientific ESCALAB 250 instrument with a monochromatic AlKα source. Raman spectrum was carried out on the Renishaw in Via Raman system 1000 with a 532 nm Nd:YAG excitation source. Diffuse reflectance spectra (DRS) were recorded on a Shimadzu-2501PC spectrometer using $BaSO_4$ as a standard. Photoluminescence spectra were measuring using a FL-2T2 instrument (SPEX, USA) with 450-W xenon lamp monochromatized by double grating (1200gr/mu). Electrochemical experiments were conducted on CHI 660B electrochemical workstation. The UV-visible adsorption spectrum was recorded using a Hitachi U-3010 UV-visible spectrometer. The conductivity measurement was performed by the conventional four-probe technique.

Synthesis of $[Zn(cca)(bipy)]_n \cdot n(bipy)$ (CP)

CP was prepared from the mixture of $Zn(OAc)_2 \cdot 4H_2O$ (0.030 g, 0.1 mmol), H_2cca (0.019 g, 0.1 mmol), bipy (0.016 g, 0.1 mmol) and H_2O (5 mL), the pH value of the mixture was adjusted to 5 with 1M NaOH. After being stirred for another 10 minutes, the mixture was transferred to a 23 mL Teflon-lined stainless steel bomb and kept at 160˚C under autogenously pressure for 5 days. A large amount of colorless crystals of **CP** were found. Yield: 82% (based on Zn). Anal. Calcd for $C_{40}H_{22}N_4O_4Zn$: C, 63.47%; H, 3.90%; N, 9.87%. Found: C, 63.65%; H, 3.79%; N, 9.93%. IR: 3208 (s), 3019 (s), 1594 (s), 1536 (s), 1012 (s), 983 (s), 869 (s), 754 (s), 464 (s).

Synthesis of CPNBs

The crystals of **CP** were grinded for 3 hours with an agate mortar and pestle. The resulted powder was dissolved in methanol and placed in a Teflon autoclave, which was heated in a microwave oven at 300 W for 3 hours. The **CPNB** was separated by centrifugation, rinsed with water and then dried in a vacuum drier at 80 ˚C for 24 hours.

Synthesis of GO

Initially, **GO** was synthesized from graphite using a modified Hummers method. 1.0 g graphite was added to 70 ml H_2SO_4 (98%) with stirring in an ice bath. Then 0.5 g $NaNO_3$ was added and stirred for 5 minutes. Consequently, a certain amount of $KMnO_4$ was added gradually to the dark mixture, and the reaction mixture was maintained at that temperature and stirred for 3 hours. After that, 70 ml deionized water and 20 mL H_2O_2 was added respectively and the resulted reaction system was maintained for 30 minutes. After the addition of hydrogen peroxide, the color of the solution turned brown, which indicated fully oxidized graphite. The as-obtained graphite oxide slurry was sonicated for 4 hours at 70 ˚C and exfoliated to generate **GO** nanosheets. At last, the mixture was separated by centrifugation, washed repeatedly with 0.5M HCl and deionized water, and dried in a vacuum oven at 60 ˚C for 24 hours. In this experiment, the mass of $KMnO_4$ is 3.0 g, 4.5 g, 6.0 g and 7.5 g. Resulted products were labeled as **GO(A)**, **GO (B)**, **GO(C)** and **GO(D)** respectively.

Synthesis of GO/CPNB and **GO/CPNBM**

The composite materials were prepared by one-step colloidal blending process using **CPNB** and **GO** in H_2O. At first, **GO** (1 mg/mL) was dissolved in 10 mL water. Then, **CPNB** (1.0 g) was dispersed in 40 mL water and dropped into the solution of **GO**. The resulted mixture was sonicated for 1 hour and further stirred for 5 hours at room temperature to obtain a homogeneous solution. The product was separated and dried in a vacuum drier at 70 ˚C for 12 hours. From **GO(A)** to **GO(D)**, the resulted composite materials were denoted as **GO(A)/CPNB**, **GO(B)/CPNB**, **GO(C)/CPNB** and **GO(D)/CPNB** respectively. **GO/CPNBM** was obtained from the mixture of **CPNB** and **GO** (with mass ration 100:1), which was grinded for 1 hour with an agate mortar and pestle. The product was separated and dried in a vacuum.

Wetting behavior test of GO

A droplet of **GO** suspension in ethanol was placed on a cleaned glass substrate fixed on a spin coater at a rotating speed of 2000 rpm for 3 minutes, and a film would be formed after drying. The wettability of the as-prepared films was characterized by measuring the water contact angle (CA) with a contact angle meter. A 2 μL water droplet was placed on this particle array film for water CA measurement. CA values were obtained by averaging five measurements on different areas of the sample surface.

Photocatalytic activity study

The photocatalytic activities of the samples were evaluated by the reduction of $K_2Cr_2O_7$ in the aqueous solution. The sample was composed of 80 ml 10 ppm $K_2Cr_2O_7$ aqueous solution and 20 mg catalysts. After the suspension containing $K_2Cr_2O_7$ and photocatalyst being magnetically stirred in dark for 40 minutes till an adsorption-desorption equilibrium was established, it was exposed to illumination. A 300 W medium pressure mercury lamp served as an ultraviolet light source and a 300 W Xe lamp with a cutoff filter ($\lambda \geq 420$ nm) served as a visible light source. Samples were then taken out regularly from the reactor and centrifuged immediately for separation of any suspended solid. The concentration of Cr(VI) was determined colorimetrically at 540 nm with diphenylcarbazide (DPC) by a UV-vis spectrometer. Langmuir-Hinshelwood (L-H) equation ($r_0 = k_0C_0/1 + K_0C_0$) was employed to quantify the reduction reaction of $Cr_2O_7^{2-}$ (r_0 represents the initial rate, k_0 represents the kinetic rate constant and K_0 represents the adsorption coefficient of the reactant $Cr_2O_7^{2-}$). As the value of C_0 is too small, $K_0C_0 \ll 1$, the L-H rate expression can be simplified to the first-order rate expression: $r_0 = dC_0/dt = k_0C_0$. This equation can be solved to obtain $\ln(C/C_0) = -k_0t$. Based on Lambert-Beer law, $C/C_0 = I/I_0$, the equation

can be reduced to $\ln(I/I_0) = -k_0t$ finally.

Electrochemical measurements

Photoelectrochemical tests were carried out with a conventional three-electrode system in quartz cell filled with 0.1 M Na_2SO_4 electrolyte (100 mL), with the **CPNB/ITO** or **GO/CPNB/ITO** serving as the working electrode, a Pt plate as the counter electrode, and a saturated calomel electrode (SCE) as the reference electrode. A 300 W Xe lamp with a cutoff filter ($\lambda \geq 420$ nm) was used as the excitation light source for visible irradiation. Electrochemical impedance spectra (EIS) were recorded in potentiostatic mode. The amplitude of sinusoidal wave was 10 mV, and the frequency of the sinusoidal wave ranged from 100 kHz to 0.05 Hz. The Mott-Schotty plot was measured at a frequency of 100 HZ in the dark.

X-ray crystallography

Suitable single crystal of **CP** was carefully selected under an optical microscope and glued on glass fiber. Structural measurement was performed on a Bruker AXS SMART APEX II CCD diffractometer at 293 K. The structure was solved by the direct method and refined by the full-matrix least-squares method on F^2 using the SHELXTL 97 crystallographic software package.[19] Anisotropic thermal parameters were used to refine all non-hydrogen atoms. Carbon-bound hydrogen atoms were placed in geometrically calculated positions; Oxygen-bound hydrogen atoms were located in the difference Fourier maps, kept in that position and refined with isotropic temperature factors. The X-ray structural analysis is listed in Table S1. Selected bond lengths and angles are listed in Table S2. Further details of the crystal structure have been deposited to the Cambridge Crystallographic Data Centre as supplementary publication, which can be obtain free of charge (CCDC 1004144). The Cambridge Crystallographic Data Centre via www.ccdc.cam.ac.uk/data_request/cif.

Structure and morphology of CPNB

Single-crystal X-ray diffraction analysis reveals there exists only one crystallographically independent Zn atom in the fundamental unit of **CP**, which adopts distorted octahedral coordination mode with four oxygen atoms from two cca ligands and two nitrogen atoms from a chelating bipy ligand. In **CP**, adjacent Zn atoms are connected by cca ligands and results in zigzag chains. To our interests, there exists strong C-H···O hydrogen bonds between neighboring chains, with C7-H7a···O1 bond distance 3.11 Å and bond angle 139.07°. This forms 2D undulating layers with additional bipy ligands dangling alternately on both sides. Besides hydrogen bond, π-π interactions are also apparent in **CP** between the 2D layers, which further extend the 2D layers to a 3D supramolecular network with 1D channel. Furthermore, there exist some guest bipy molecules reside in this channel (Fig. 1a). TGA illustrates CP keeps stable at 300 ˚C (Fig. S1). The morphology of **CPNB** is studied with SEM (Fig. 1b). It could be observed the lengths and widths vary from 6 to 10 μm and 1 to 3 μm, respectively. The thickness of **CPNB** can also be measured clearly, which ranges from 40 to 60 nm. Furthermore, the surface of **CPNB** seems very smooth.

Morphology and structure of GO

For **GO**, the number of functional group has great effect on photocatalytic property of **GO/CPNB** composite material. Here, this factor is controlled by the mass of $KMnO_4$ used in synthesis process of **GO**. Although morphologies of **GO** are similar, their surface element contents are of great difference (Fig. 2). The discrepancy of functional groups can be illustrated clearly from surface wettabilities. The contact angles (CA) of **GO** are 47.4°, 40.8°, 34.9° and 28.6° respectively (Fig. 2, inset). The decreasing of CA illustrates with addition of $KMnO_4$, the number of functional group

increases and hydrophilic property of **GO** is improved. This will initiate supramolecular interactions (such as hydrogen bonds and π-π interactions) and the synergy effect between **CPNB** and **GO**.

To study the structure of **GO** in detail, XPS and Raman spectra were employed (Fig. 3). In **GO**, the peaks appear at 532.3 and 284.7 eV can be ascribed to O1s and C1s respectively. C 1s spectra reveal there exist three kinds of carbon bonds in **GO**, which are C-C (284.8 eV), -C=O (287.6 eV) and -COOH (289.2 eV) respectively (Fig. S2a to 2d).[20] This can also be confirmed by O 1s spectra (Fig. S2e to 2h). Furthermore, from **GO(A)** to **GO(D)**, the intensity ratio between O1s and C1s peaks increase slowly, which indicates the increasing of functional groups on surface of **GO** (Fig. S2i to 2l). The results of Raman spectra also suggest this point (Fig. S3). For **GO**, its D and G bands can be assigned to the defects or disordering atomic arrangement of sp^3 hybridized carbon atoms and plane vibration sp^2 hybridized carbon atoms in 2D layer of **GO** respectively.[21] So the higher I_D/I_G value can indicates more defects and disorders exist on the **GO**. From **GO(A)** to **GO(D)**, the I_D/I_G value increases from 1.05 to 1.19, which further indicates the addition of functional groups on the surface of **GO** with the increasing of $KMnO_4$.

Morphology and structure of GO/CPNB composite materials

The morphologies of **GO/CPNB** were studied with SEM (Fig. 3). It can be seen obviously **GO** coats eventually on the surface of **CPNB**. In these composite materials, **CPNB** exhibit similar dimension and element content with pure **CPNB**. PXRD was applied to study structures of **CPNB** and **GO/CPNB**. **CPNB** and **GO/CPNB** both exhibit similar diffraction patterns with **CP**, which illustrates in **CPNB** and **GO/CPNB** the structure of **CP** is well retained (Fig. S4a and 4b). Furthermore, the peaks belonging to **GO** are not observed, which can be ascribed to the content of **GO**

may be too small to determine its existence (Fig. S4c). To study the interactions between **CPNB** and **GO**, FTIR spectra were employed. For **CPNB**, the peaks appearing at about 1594 to 1536 cm^{-1} can be ascribed to the asymmetric and symmetric stretching vibrations of carboxlyate groups in the cca ligand (Fig. S4d and 4e). Compared with **CPNB**, in the **GO/CPNB**, these peaks shift to a higher wavenumber region (Fig. S4f). The movements reveal the effective interactions between **CPNB** and **GO**, which can be ascribed to the existence of hydrogen bond or π-π interaction.[22]

The structures of **GO/CPNB** composite materials were investigated in detail with XPS (Fig. 4). **CPNB** shows two peaks located at 1022.2 and 1045.2 eV, which are assigned Zn $2p_{3/2}$ and Zn $2p_{1/2}$ respectively. From **GO(A)/CPNB** to **GO(D)/CPNB**, the Zn $2p_{3/2}$ and Zn $2p_{1/2}$ peaks shifted to higher energy levels and appeared at 1024.9, 1048.8 eV; 1025.1, 1048.2 eV; 1025.3, 1048.3 eV and 1024.8, 1047.9 eV respectively. The movements of these peaks can be attributed to the generation of Zn-O bonds between **CPNB** and **GO**. Because compared with zinc, carbon is a highly electronegative element, which can withdraw the electron from Zn.[17a] As a result, compared with Zn in **CPNB**, the binding energy of Zn increases in **GO/CPNB** composite materials.

Optical and electrochemical analysis

The diffuse reflectance spectra (DRS) of **CPNB** and **GO/CPNB** composite materials were studied. Compared with **CPNB**, composite materials exhibit much stronger absorptions in visible light region, which suggest the coating of **GO** on **CPNB** is a feasible strategy to improve its photoresponse in visible light region (Fig. 5a). To illustrate this point in detail, band gaps (E_g) of **CPNB** and **GO/CPNB** were obtained from Tauc equation. From **GO(A)/CPNB** to **GO(D)/CPNB**, band gaps are

2.79, 2.62, 2.32 and 2.41 eV respectively, while for **CPNB**, its band gap is 3.65 eV, which is much wider than above composite materials. This further indicates **CPNB** is active only in ultraviolet light region, while **GO/CPNB** composite materials can be irradiated in both ultraviolet and visible light region. To clarify the fate of electron and hole, photoluminescence spectra was employed (Fig. 5b). For **CPNB**, the main emission peak appears at 480 nm, which can be ascribed to π-π* or π-n transitions of cca ligand.[23] Furthermore, the emission intensity of **CPNB** is strong, which illustrates after irradiation, a large amount of electrons and holes recombine and result in photoluminescence.[24] On the contrary, the photoluminescence of composite materials is much weaker than **CPNB**; in particular, **GO(C)/CPNB** gives the lowest photoluminescence intensity among these four composite materials. This results indicate the coating of **GO** on **CPNB** is an effective strategy to impede the recombination of electron and hole.

The optical research results are also supported by electrochemical analysis. Here, the interface charge separation efficiency was investigated by photocurrent spectra (Fig. 5c). Under visible light irradiation, **CPNB** is inactive, while for **GO/CPNB**, upon irradiation, the photocurrent appeared promptly and then reached a relatively steady state, when the illumination was shut down, the current fell to zero immediately. Furthermore, their reproducibility and stability are excellent as the illumination was turned on and off. The highest photocurrent was achieved with **GO(C)/CPNB**, which is about one and an half times than **GO(A)/CPNB**. To study the charge separation and transfer process in detail, EIS was employed (Fig. 5d). The typical EIS spectra were presented as Nyquist plots. It can be observed obviously, the introduction of **GO**, through in small amount, is able to lead to dramatic decrease in *arc* radiuses as compared with **CPNB**. This indicated a decrease in the solid state

interface layer resistance and the charge transfer resistance of the surface, which facilitates the transportation of electron and impede its recombination with hole.[25]

Based on optical and electrochemical analysis results, extension of photoresponse region as well as enhancement of electron-hole pair separation efficiency both benefit from the introduction of **GO**. However, excessive increasing of functional groups on **GO** exhibits a negative effect on the efficiency of photocatalyst.

Photocatalytic property study

The photocatalytic reduction of $Cr_2O_7^{2-}$ over **CPNB** and **GO/CPNB** composite materials were evaluated (Table 1). Compare with visible light inactive **CPNB**; composite materials exhibit more excellent photocatalytic activities under irradiation of visible light (Fig. S5). Moreover, it is clear, for **GO**, the number of functional groups exhibits great influence on photocatalytic efficiency of **GO/CPNB** composite materials. As functional groups increased, photocatalytic activity of composite material does not raise monotonously (Fig. 6a). The reason for this tendency can be explained as follows: with the increasing of functional group, **GO** is coated on **CPNB** more tightly, so the transportation of electron is speeded up and electron-hole pair can be separated more adequately, which enhances the photocatalytic efficiency of the photocatalyst. But as functional group raise continually, more defects may appear on its surface, the extensively conjugated π system and layer structure can be damaged. This will decrease electron transportation property of **GO** and impede the separation of electron-hole pair, which stems further enhancement of photocatalytic efficiency. The suggestion is proved to be truth by the conductivity of **GO** (Fig. 6b). For a photocatalyst, during photocatalytic reduction of $Cr_2O_7^{2-}$, the repeatability and stability are crucial factors for its practical applications. For **GO(C)/CPNB**, after recycled for five times, the activity only decreased about 3%, which indicates it

possessed favorable recycling property (Fig. 6c). Moreover, **GO(C)/CPNB** also displayed excellent stability during reduction of $Cr_2O_7^{2-}$, which was confirmed by PXRD pattern and FTIR (Fig. 6d and 6e). This indicates the structure of **GO(C)/CPNB** is not destroyed during the reduction process of Cr(VI).

In composite materials, the improvement of photocatalytic activity originates from the synergy between **GO** and **CPNB**. To illustrate this point clearly, **GO/CPNBM** (the mechanically blended product of **GO** and **CPNB**) were used as the reference to evaluate the photocatalytic efficiency (Fig. 6f). It is notable that their photocatalytic efficiency is considerably less than **GO/CPNB**. This result indicates that the synergy between **GO** and **CPNB** plays the dominating role in the enhancement of photocatalytic activity. The synergy is introduced by supramolecular interaction between **GO** and **CPNB**, which facilitates the transportation of photogenerated electron and achieve efficient separation of hole and electron. To quantify the extent of synergy effect between **GO** and **CPNB**, a parameter, named as synergy factor (R) was introduced, which is defined as $k_{GO/CPNB}/k_{GO/CPNBM}$. From **GO(A)/CPNB** to **GO(D)/CPNB**, R values are 1.55, 1.95, 4.56 and 2.63 respectively, which suggests the coating of **GO** on **CPNB** does create an obvious synergetic effect in composite material. In these composite materials, synergetic effect of **GO(C)/CPNB** is the most obvious and this lies in the particular structural feature of **GO(C)**.

Mechanism study

For **GO/CPNB** composite material, to illustrate the reason why its photocatalytic activity is improved so greatly, the analysis of **CPNB**'s energy bands is necessary. The conductive band (CB) potential of **CPNB**, obtained with Mott-Schotty measurement is -0.65 eV (vs SCE) and the positive slope of C^{-2}/E plot illustrates **CPNB** is a typical n-type semiconductors.[26] Based on its band gap, with the formula

$E_{VB} = E_{CB} + E_g$, valence band (VB) of **CPNB** is calculated to be 3.00 eV (vs SCE) (Fig. 7a). For **GO**, its Fermi energy level is higher than CB edge of **CPNB**, so after the coating of **GO** on **CPNB**, a new energy level is formed between the **CPNB**'s CB and Fermi energy level of **GO**, which can be considered as the CB of **GO/CPNB**.[27] During this process, the VB energy level of **CPNB** is retained. This leads to the decreasing of band gap in the resulted composite material (Fig. 7b). So, under visible light, composite material can be excited and produce electron on VB of **CPNB**. Subsequently, electron injects to the CB of **CPNB** and then transferred to **GO**. Simultaneously, positive charged holes are formed on VB of **CPNB**. Thus the photogenerated electron-hole pair can be separated adequately and the recombination of electron and hole is reduced or inhabited. This enhances the efficiency of interfacial charge transfer to $Cr_2O_7^{2-}$ and accelerates its reduction reaction.

Conclusions

In summary, the wide responsive photocatalyst, **GO/CPNB** was successfully prepared with a facile colloidal blending process under mild conditions. The investigation of its photocatalytic activity exhibits **GO/CPNB** composite material possesses much better photocatalytic efficiency for the reduction of $Cr_2O_7^{2-}$ than **CPNB**, **GO** and their mechanical blended mixture. XPS illustrates **CPNB** is coated on **GO** through chemical bonds between Zn and functional groups on its surface. The formation of these bonds results in composite material with lower band gap and wide photoresponse region. Furthermore, this combination also leads to the generation of synergistic effect between **CPNB** and **GO**, which enhances the separation of photogenerated carrier and improve the photocatalytic efficiency. It has been demonstrated that **GO/CPNB** can be used in the treatment of Cr(VI) containing wastewater in industrial production. Moreover, the visible light driven photocatalytic

activity and excellent stability also render it to be a promising photoelectric conversion material with good potential applications in hydrogen production by sufficiently utilizing solar energy.

Acknowledgements

This work was supported by Province Nature Sciences Foundation of Liaoning Province (201102166) and National Natural Science Foundation of China (21303010).

Electronic supplementary information (ESI) available: Crystal data and structure refinement results, selected bond lengths and angles of **CP**; PXRD and FTIR patterns of **CPNB** and **GO/CPNB**; Reduction rate as the function of time by **CPNB** under UV light.

Reference

1 (a) M. Gheju, A. Iovi and I. Balcu, *J. Hazard. Mater*., 2008, **153**, 655; (b) Y. Gong and X. Liu, *J. Hazard. Mater*., 2010, **179**, 540; (c) R. J. Kieber, J. D. Willey and S. D. Zvalaren, *Environ. Sci. Technol*., 2002, **36**, 5321; (d) N. Shevchenko, V. Zaitsev and A. Walcarius, *Environ. Sci. Technol*., 2008, **42**, 6922.

2 (a) R. L. Qiu, D. D. Zhang, Z. H. Diao, X. F. Huang, C. He, J. L. Morel and Y. Xiong, *Water Res*., 2012, **46**, 2299; (b) M. V. Dozzi, A. Saccomanni and E. Selli, *J. Hazard. Mate*r., 2012, **211**, 188; (c) M. Rivero and W. D. Marshall, *J. Hazard. Mater*., 2009, **169**,1081; (d) L. M. Wang, N. Wang, L. H. Zhu, H. W. Yu and H. Q. Tang, *J. Hazard. Mater*., 2008, **152**, 93; (e) J. M. Meichtry, M. Brusa, G. Mailhot, M. A. Grela and M. I. Litter, *Appl. Catal. B*, 2007, **71**, 101.

3 (a) H. L. Ma, Y. W. Zhang, Q. H. Hu, D. Yan, Z. Z. Yu and M. L. Zhai, *J. Mater. Chem*., 2012, **22**, 5914; (b) G. Liu, Q. Deng, H. M. Wang, S. H. Kang, Y. Yang, D. H. L. Ng, W. P. Cai and G. Z. Wang, *Chem.-Eur. J*., 2012, **18**, 13418; (c) T. J. Yao, T. Y. Cui, J. Wu, Q. Z. Chen, S. W. Lu and K. N. Sun, *Polym. Chem*., 2011, **2**, 2893; (d) Y. Cheng, F. Yan, F. Huang, W. Chu, D. Pan, Z. Chen, J. Zheng, M. Yu, Z. Lin and Z. Wu, *Environ. Sci. Technol*., 2010, **44**, 6357.

4 (a) X. J. Liu, L. K. Pan, T. Lv, G. Zhu, T. Lu, Z. Sun and C. Q. Sun, *RSC Adv*., 2011, **1**, 1245; (b) I. Heidmann and W. Calmano, *J. Hazard. Mater*., 2008, **152**, 934; (c) J. W. Fan, X. H. Liu and J. Zhang, *Environ. Technol*., 2011, **32**, 427; (d) X. F. Sun, Y. Ma, X. W. Liu, S. G. Wang, B. Y. Gao and X. M. Li, *Water Res*., 2010, **44**, 2517; (e) Y. Q. Xing, X. M. Chen and D. H. Wang, *Environ. Sci. Technol*., 2007, **41**, 1439.

5 (a) H. Yoneyama, Y. Yamashita and H. Tamura, *Nature* 1979, **281**, 817; (b) B. Saha and C. Orvig, *Coord. Chem. Rev*., 2010, **254**, 2959; (c) S. Sajjad, S. A. K. Leghari,

F. Chen and J. L. Zhang,*Chem.-Eur. J.*, 2010, **16**, 13795; (d) M. Gheju and I. Balcu, *J. Hazard. Mater.*, 2011, **196**, 131; (e) S. E. Fendorf and R. Zasoski, *Environ. Sci. Technol.*, 1992, **26**, 79.

6 (a) A. Tanaka, K. Nakanishi, R. Hamada, K. Hashimoto and H. Kominami, *ACS Catal.*, 2013, **3**, 1886; (b) X. H. Gao, H. B. Wu, L. X. Zheng, Y. J. Zhong, Y. Hu and X. W. Lou, *Angew. Chem. Int. Ed.*, 2014, **53**, 5917; (c) D. K. Padhi and K. Parida, *J. Mater. Chem. A*, 2014, **2**, 10300.

7 (a) L. J. Shen, S. Liang, W. M. Wu, R. W. Liang and L. Wu, *J. Mater. Chem. A*, 2013, **1**, 11473; (b) Y. Horiuchi, T. Toyao, M. Takeuchi, M. Matsuoka and M. Anpo, *Phys. Chem. Chem. Phys.*, 2013, **15**, 13243; (c) Y. Q. Chen, G. R. Li, Y. K. Qu, Y. H. Zhang, K. H. He, Q. Guo and X. H. Bu, *Cryst. Growth Des.*, 2013, **13**, 901; (d) L. J. Shen, W. M. Wu, R. W. Liang, R. Lin and L. Wu, *Nanoscale* 2013, **5**, 937.

8 (a) C. F. Zhang, L. G. Qiu, F. Ke, Y. J. Zhu, Y. P. Yuan, G. S. Xu and X. Jiang, *J. Mater. Chem. A*, 2013, **1**, 14329; (b) W. W. Zhan, Q. Kuang, J. Z. Zhou, X. J. Kong, Z. X. Xie and L. S. Zheng, *J. Am. Chem. Soc.*, 2013, **135**, 1926; (c) Y. Q. Chen, S. J. Liu, Y. W. Li, G. R. Li, K. H. He, Y. K. Qu, T. L. Hu and X. H. Bu, *Cryst. Growth Des.*, 2012, **12**, 5426; (d) Z. Q. Li, A. Wang, C. Y. Guo, Y. F. Tai and L. G. Qiu, *Dalton Trans.*, 2013, **42**, 13948; (e) J. L. Wang, C. Wang and W. B. Lin, *ACS Catal.*, 2012, **2**, 2630.

9 (a) Y. H. Fu, D. R. Sun, Y. J. Chen, R. K. Huang, Z. X. Ding, X. Z. Fu and Z. H. Li, *Angew. Chem., Int. Ed.*, 2012, **51**, 3364; (b) H. Khajavi, J. Gascon, J. M. Schins, L. D. A. Aiebbeles and F. Kapteijn, *J. Phys. Chem. C*, 2011, **115**, 12487; (c) C. G. Silva, A. Corma and H. García, *J. Mater. Chem.*, 2010, **20**, 3141; (d) P. Mahata, C. Madras and S. Natarajan, *J. Phys. Chem. C*, 2006, **110**, 13759.

10 (a) M. C. Das, H. Xu, Z. Y. Wang, G. Srinivas, W. Zhou, Y. F. Yue, V. N. Nesterov, G. D. Qian and B. L. Chen, *Chem. Commun*., 2011, **47**, 11715; (b) C. Wang, Z. G. Xie, K. E. DeKrafft and W. B. Lin, *J. Am. Chem. Soc*., 2011, **133**, 13445; (c) C. G. Silva, I. Luz, F. X. L. Xamena, A. Corma and H. García, *Chem.-Eur. J*., 2010, **16**, 11133; (d) T. Tachikawa, J. R. Choi, M. Fujitsuka and T. Majima, *J. Phys. Chem. C*, 2008, **112**, 14090.

11 (a) L. J. Shen, S. Liang, W. M. Wu, R. W. Liang and L. Wu, *Dalton Trans*., 2013, **42**, 13649; (b) K. X. Wang and J. S. Chen, *Acc. Chem. Res*., 2011, **44**, 531; (c) Z. T. Yu, Z. L. Liao, Y. S. Jiang, G. H. Li and J. S. Chen, *Chem.-Eur. J*., 2005, **11**, 2642. (d) Z. T. Yu, Z. L. Liao, Y. S. Jiang, G. H. Li, G. D. Li and J. S. Chen, *Chem. Commun*., 2004, 1814.

12 (a) P. Y. Wu, C. He, J. Wang, X. J. Peng, X. Z. Li, Y. L. An and C. Y. Duan, *J. Am. Chem. Soc*., 2012, **134**, 14991; (b) F. Wang, X. H. Ke, J. B. Zhao, K. J. Deng, X. K. Leng, Z. F. Rian, L. L. Wen and D. F. Li, *Dalton Trans*., 2011, **40**, 11856; (c) D. E. Wang, K. J. Deng, K. L. Lv, C. G. Wang, L. L. Wen and D. F. Li, *CrystEngComm*., 2009, **11**, 1442; (d) L. L. Wen, F. Wang, J. Feng, K. L. Lv, C. G. Wang and D. F. Li, *Cryst. Growth Des*., 2009, **9**, 3581.

13 (a) S. Sakthivel and H. Kisch, *Angew. Chem. Int. Ed*., 2003, **42**, 4908; (b) D. L. Zhao, G. D. Sheng, C. L. Chen and X. K. Wang, *Appl. Catal. B*, 2012, **111-112**, 303; (c) Y. Y. Liang, H. L. Wang, H. S. Casalongue, Z. Chen and H. J. Dai, *Nano Res*., 2010, **3**, 701; (d) C. L. Lin, Y. H. Cheng, Z. X. Liu and J. Y. Chen, *J. Hazard. Mater*., 2011, **197**,254; (e) L. Zhang, Q. Zhou, J. Y. Liu, N. Chang, L. H. Wan and J. H. Chen, *Chem. Eng. J*., 2012, **185-186**, 160; (f) K. Dai, T. Y. Peng, D. N. Ke and B. Q. Wei, *Nanotechnology* 2009, **20**, 125603.

14 (a) W. Sun, M. Chen, S. X. Zhou and L. M. Wu, *J. Mater. Chem. A*, 2014, **2**,

14004; (b) X. Q. An, J. C. Yu and J. M. Tang, *J. Mater. Chem. A*, 2014, **2**, 1000; (c) B. Weng, M. Q. Yang, N. Zhang and Y. J. Xu, *J. Mater. Chem. A*, 2014, **2**, 9380; (d) J. H. Byeon and J. M. Kim, *J. Mater. Chem. A*, 2014, **2**, 6939.

15 (a) M. S. A. S. Shah, A. R. Park, K. Zhang, J. H. Park and P. J. Yoo, *ACS Appl. Mater. Interfaces* 2012, **4**, 3893; (b) W. J. Ren, Z. H. Ai, F. L. Jia, L. Z. Zhang, X. X. Fan and Z. G. Zou, *Appl. Catal. B*, 2007, **69**, 138. (c) Y. Zhao, D. L. Zhao, C. L. Chen and X. K. Wang, *J. Colllid Interface Sci*., 2013, **405**, 211.

16 (a) Q. J. Xiang, J. G. Yu, M. Jaroniec, *Chem. Soc. Rev*, 2012, 41, 782. (b) H. Zhang, X. J. Lv, Y. Wang and J. H. Li, *ACS nano*., 2010, **4**, 380.

17 (a) C. Petit and T. J. Bandosz, *Adv. Funct. Mater*., 2010, **20**, 111; (b) C. Petit and T. J. Bandosz, *Adv. Funct. Mater*., 2011, **21**, 2108; (c) C. Petit and T. J. Bandosz, *Adv. Mater*., 2009, **21**, 4753; (d) J. H. Lee, S. Kang, J. Jaworski, K. Y. Kwon, M. L. Seo, J. Y. Lee and J. H. Jung, *Chem.-Eur. J*., 2012, **18**, 765.

18 (a) Q. J. Xiang, J. G. Yu and M. Jaroniec, *Chem. Soc. Rev.,* 2012, **41**, 782; (b) P. Kumar, B. Sain and S. L. Jain, *J. Mater. Chem. A*, 2014, **2**, 11246; (c) L. Yan, M. Q. Yang and Y. J. Xu, *J. Mater. Chem. A*, 2014, **2**, 14401; (d) Z. G. Xiong, H. Wu, L. H. Zhang, Y. Gu and X. S. Zhao, *J. Mater. Chem. A*, 2014, **2**, 9291.

19 (a) G. M. Sheldrick, *SHELX-97, Program for Crystal Structure Refinement*, University of Göttingen, Germany, 1997; (b) G. M. Sheldrick, *SHELX-97, Program for Crystal structure Solution*, University of Göttingen, Germany, 1997.

20 (a) T. J. Bandosz, E. Rodríguez-Castellón, J. M. Montenegro and M. Seredych, *Carbon* 2014, **77**, 651; (b) C. Ania, M. Seredych, E. Rodríguez-Castellón and T. J. Bandosz, *Carbon* 2014, **79**, 432; (c) L. F. Velasco, J. C. Lina and C. Ania, *Angew. Chem. Int. Ed*., 2014, **53**, 4146.

21 (a) Y. Zhang, Z. Tang, X. Fu and Y. Xu, *ACS Nano*., 2011, **5**, 7426; (b) O.

Akhavan, *ACS Nano*., 2010, **4**, 4174; (c) O. Akhavan, M. Abdolahad, A. Esfandiar and M. Mohatashamifar, *J. Phys. Chem. C*, 2010, **114**, 12955.

22 (a) J. H. Wei, Q. Zhang, Y. Liu, R. Xiong, C. X. Pang and J. Shi, *J. Nanopart. Res*., 2011, **15**, 3157; (b) L. X. Zhang, P. Liu and Z. X. Su, *Polym. Degrad. Stab*., 2006, **91**, 2213; (c) S. X. Min, F. Wang and Y. Q. Han, *J. Mater Sci*., 2007, **42**, 9966.

23 (a) Z. Su, J. Fan, M. Chen, T. Okamura and W. Y. Sun, *Cryst. Growth Des*., 2011, **11**, 1159; (b) B. Wu, Z. G. Ren, H. X. Li, M. Dai, D. X. Li, Y. Zhang and J. P. Lang, *Inorg. Chem. Commun*., 2009, **12**, 1168.

24 (a) A. C. Arango, S. A. Carter and P. J. Brock, *Appl. Phys. Lett*., 1999, **74**, 1698; (b) L. Song, R. L. Qiu, Y. Q. Mo, D. D. Zhang, H. Wei and Y. Xiong, *Catal Commun*., 2007, **8**, 429; (c) J. S. Salafsky, W. H. Lubberhuizen and R. E. I. Schropp, *Chem. Phys. Lett*., 1998, **290**, 297.

25 (a) W. H. Leng, Z. Zhang, J. Q. Zhang and C. N. Cao, *J. Phys. Chem. B*, 2005, **109**, 15008; (b) H. Liu, S. A. Cheng, M. Wu, H. J. Wu, J. Q. Zhang, W. Z. Li and C. N. Cao, *J. Phys. Chem. A*, 2000, **104**, 7016.

26 (a) X. H. Lu, G. M. Wang, S. L. Xie, J. Y. Shi, W. Li, Y. X. Tong and Y. Li, *Chem. Commun*., 2012, **48**, 7717; (b) L. J. Shen, S. J. Liang, W. M. Wu, R. W. Liang and L. Wu, *Dalton Trans*., 2013, **42**, 13649; (c) L. H. Ai, C. H. Zhang, L. L. Li and J. Jiang, *Appl. Catal. B*, 2014, **148-149**, 191.

27 (a) X. Guo, G. T. Fei, H. Su and L. D. Zhang, *J. Phys. Chem. C*, 2011, **115**, 1608; (b) M. Sun, Q. Yan, T. Yan, M. M. Li, D. Wei, Z. P. Wang, Q. Wei and B. Du, *RSC. Adv.*, 2014, **4**, 31019.

Table 1 Values of reduction efficiency (η), rate constant (k_0) of $Cr_2O_7^{2-}$ with different photocatalysts and synergy factor (R) of **GO/CPNB** composite materials.

Photocatalyst	Condition	T (min)	η (%)	k_0 (min^{-1})	R^2 (%)	R
CPNB	UV	360	67.05	0.0031	99.968	-
CPNB	Vis	360	3.24	-	-	-
GO(A)/CPNB	Vis	360	67.51	0.0031	99.976	1.55
GO(B)/CPNB	Vis	360	77.32	0.0041	99.989	1.95
GO(C)/CPNB	Vis	180	85.42	0.0105	99.844	4.56
GO(D)/CPNB	Vis	270	83.26	0.0063	99.246	2.63
GO(A)/CPNBM	Vis	360	51.48	0.0020	99.995	-
GO(B)/CPNBM	Vis	360	53.08	0.0021	99.788	-
GO(C)/CPNBM	Vis	360	54.36	0.0023	99.997	-
GO(D)/CPNBM	Vis	360	56.69	0.0024	99.991	-

Figure Captions

Figure 1 (a) 3D supramolecular network of **CP**; (b) SEM and EDX (inset) of **CPNB**.

Figure 2 SEM and the shape of a water droplet on the surface (inset): (a) **GO(A)**; (b) **GO(B)**; (c) **GO(C)**; (d) **GO(D)**.

Figure 3 SEM and EDX of **CPNB** in composite material (inset) (a) **GO(A)/CPNB**; (b) **GO(B)/CPNB**; (c) **GO(C)/CPNB**; (d) **GO(D)/CPNB**.

Figure 4 XPS of Zn and XPS survey (inset) (a) **CPNB**; (b) **GO(A)/CPNB**; (c) **GO(B)/CPNB**; (d) **GO(C)/CPNB**; (e) **GO(D)/CPNB**.

Figure 5 (a) DRS and Tauc plots (inset) of **CPNB** and **GO/CPNB**; (b) Photoluminescence spectra of **CPNB** and **GO/CPNB**; (c) Photocurrent spectra of **CPNB** and **GO/CPNB**; (d) Nynquist plots of **CPNB** and **GO/CPNB**.

Figure 6 (a) Reduction rate as the function of time by **CPNB** and **GO/CPNB**; (b) Conductivity of **GO**; (c) Cycling runs of the reduction of $Cr_2O_7^{2-}$ in the presence of **GO(C)/CPNB**; (d) PXRD of recycled **GO(C)/CPNB**; (e) FTIR of recycled **GO(C)/CPNB**; (f) Reduction rate as the function of time by **GO/CPNBM**.

Figure 7 (a) Mott-Schotty plot of **CPNB**; (b) Diagram of the photocatalytic mechanism for **GO/CPNB** under visible light.

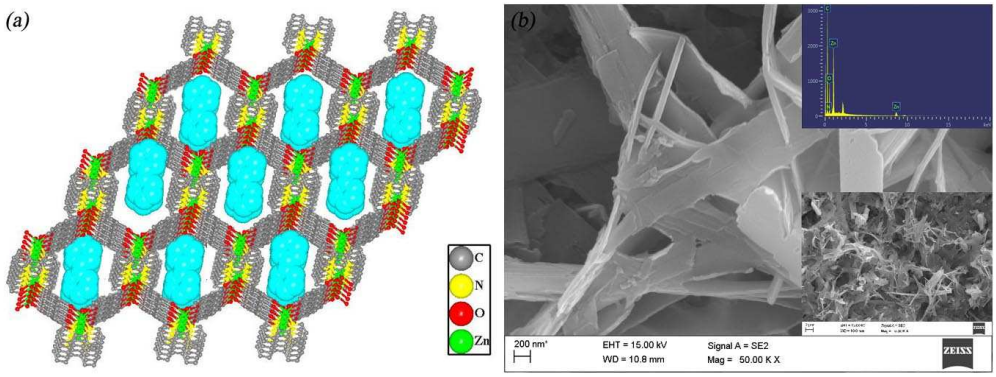

Figure 1

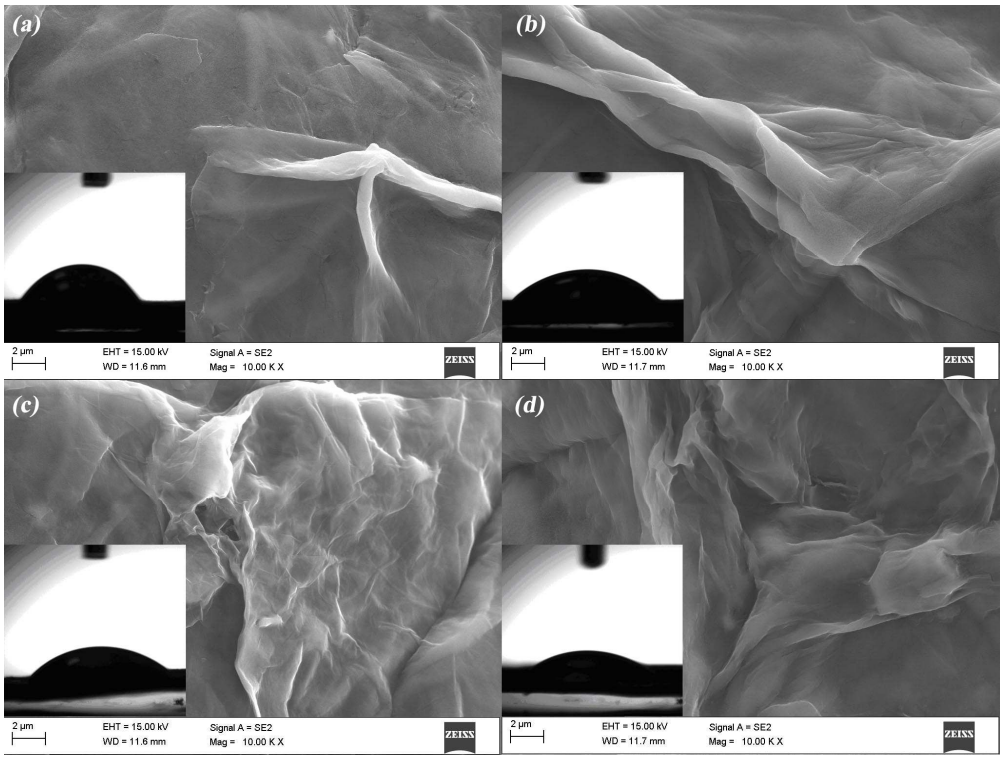

Figure 2

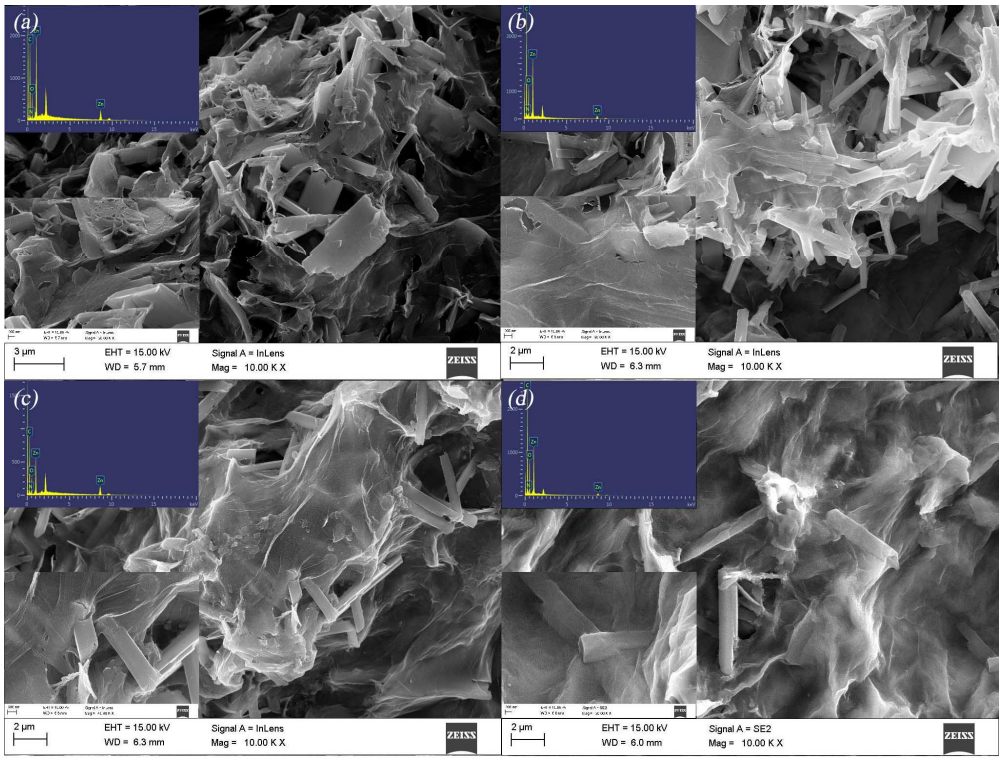

Figure 3

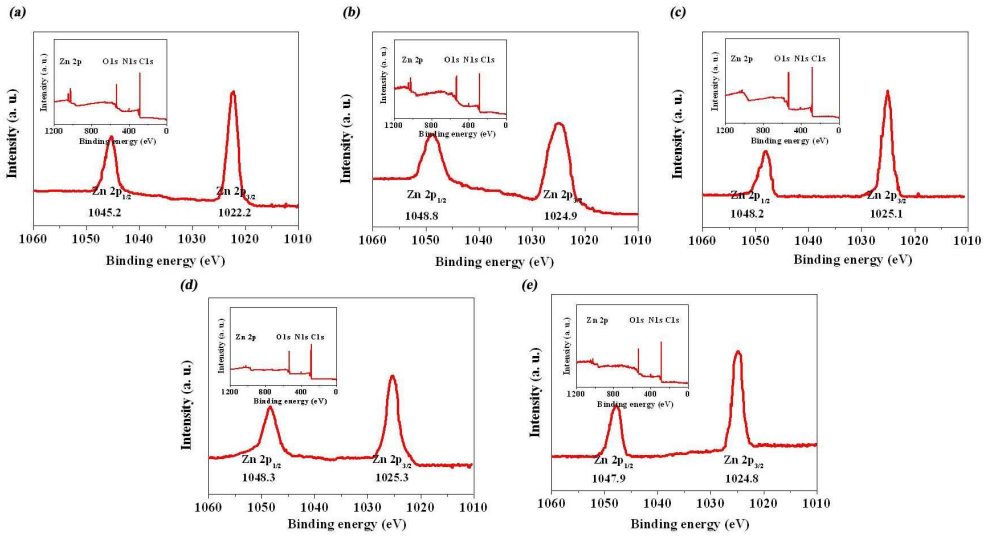

Figure 4

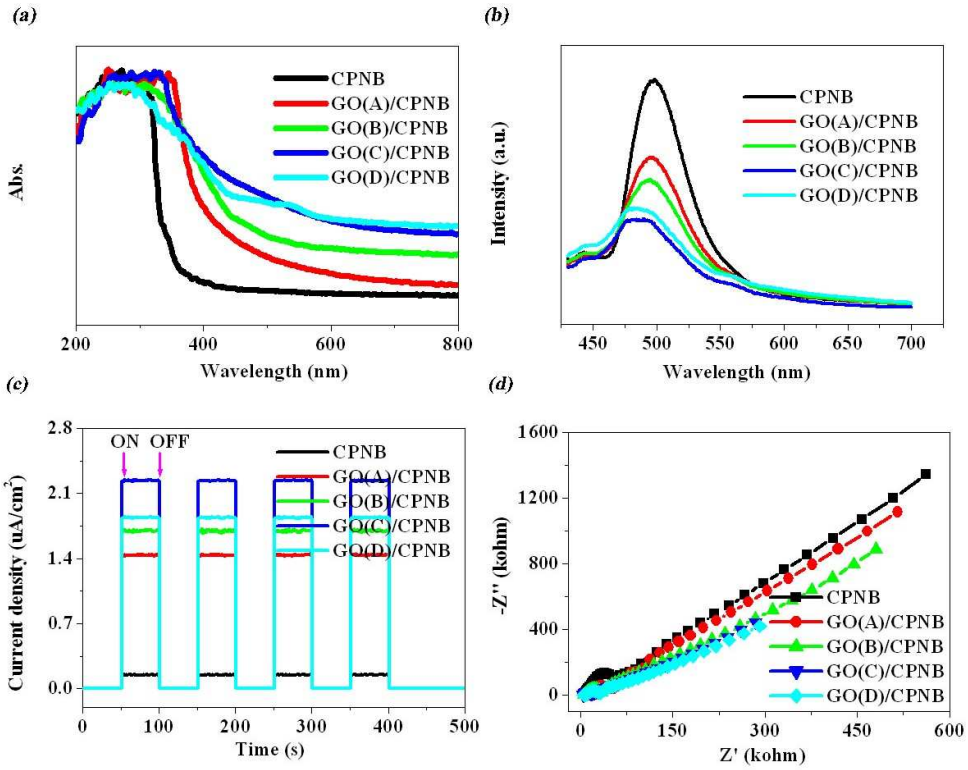

Figure 5

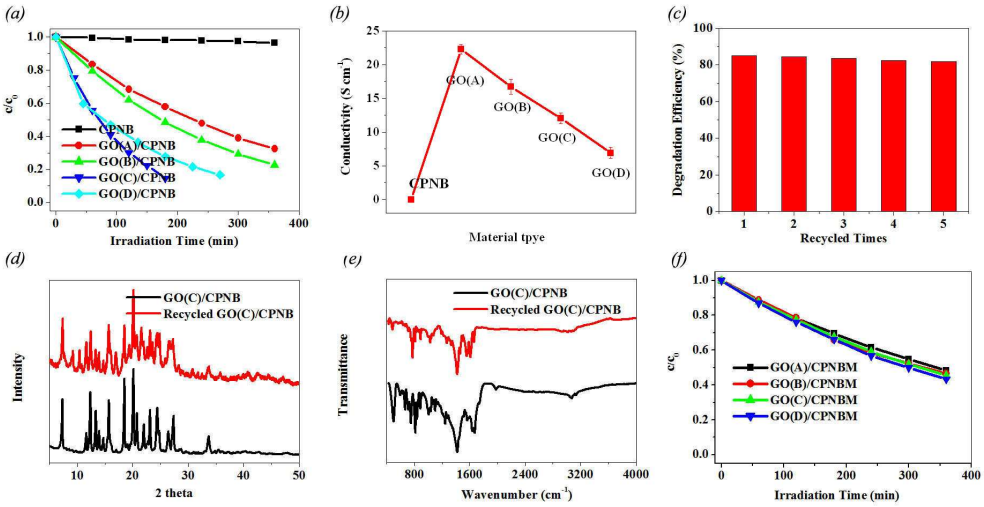

Figure 6

1

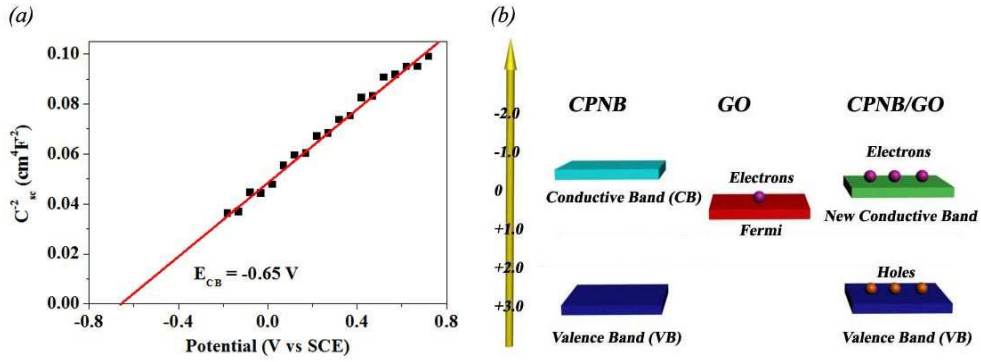

2

3 **Figure 7**

Graphical Abstract

Graphene Oxide Coated Coordination Polymer Nanobelt Composite Material: a New Kind of Visible Light Active and High Efficient Photocatalyst for Cr (VI) Reduction

Gui-Mei Shi,*[a] Bin Zhang,[a] Xin-Xin Xu,*[b] and Fu-Yang Hong[a]

[a]*College of Science, Shenyang University of Technology, No.111, Shenliao West Road, Economic & Technological Development Zone, Shenyang,110870,P. R. China*

[b] *Department of Chemistry, College of Science, Northeast University, Shenyang, Liaoning, 110819, People's Republic of China*

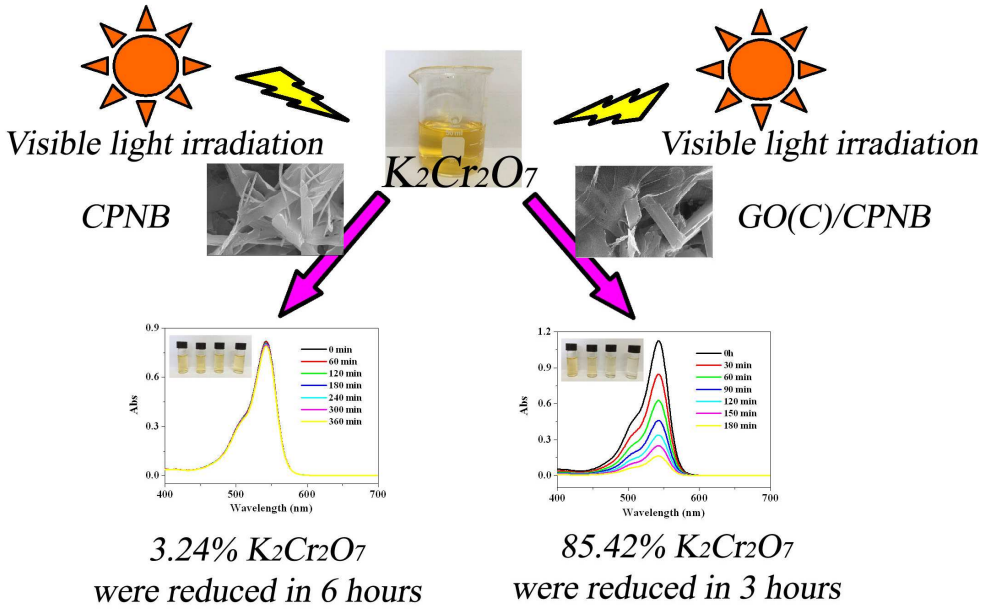

GO/CPNB was fabricated successfully, which displays very excellent photocatalytic activity in visible light. Furthermore, the influence of **GO** on photocatalytic activity was discussed.